EXPLORATION OF HEAT-INDUCED COLOR FORMATION ON NICKEL

A Thesis

by

OMAR GARZA

Submitted to the Graduate and Professional School of
Texas A&M University
in partial fulfillment of the requirements for the degree of

MASTER OF SCIENCE

Chair of Committee,	Alex (Gwo-Ping) Fang
Committee Members,	Hong Liang
	Mathew Kuttolamadom
Head of Department,	Reza Langari

December 2022

Major Subject: Engineering Technology

ABSTRACT

In this research, various pure nickel and electroless nickel-plated samples were heat treated in a regular air atmosphere at different temperatures and times to explore their heat-induced color formation effects for decorative applications. This color formation is an effect of thin-film interference between the nickel and its resulting oxide layer after heat treatment causing various colors from straw, brown, reddish-brown, purple, and blue. Control of the color formation has the potential for commercialization as a decorative method for electroless nickel-plated material. Initial experiments attempted duplicating the color formation shown on heat-treated electroless nickel-plated diamond particles. Later experiments explored the effect of how different substrates of electroless nickel-plated samples led to different color formation kinetics with Energy Dispersive X-Ray analysis. Thin film interference calculations were also compared to oxidized pure nickel samples whose oxide layer was measured by Ellipsometry and Focused Ion Beam-Scanning Electron Microscopy. Lastly, the phosphorous content produced by five different electroless nickel plating recipes on pure nickel samples was measured with an Energy Dispersive X-Ray showing a correlation related to their color formation kinetics. The same samples were also analyzed with a NIX Color Sensor, which measured their red, green, and blue color values.

DEDICATION

This work is dedicated to my mother and father, who have supported and inspired me to do more than I thought I could. Additionally, I dedicate this work to my siblings and close friends, who have added guidance and direction throughout my life.

ACKNOWLEDGMENTS

I want to thank my committee chair, Dr. Alex Fang, and my committee members, Dr. Mathew Kuttolamadom and Dr. Hong Liang, for their guidance and support throughout this research and Dr. Jorge Leon for the opportunity to pursue graduate studies.

Thanks to my friends, colleagues, and the Engineering Technology and Industrial Distribution department faculty and staff for making my time at Texas A&M University a great experience.

Finally, thanks to my mother and father for their encouragement, patience, and support.

CONTRIBUTORS AND FUNDING SOURCES

The research efforts were supervised by a thesis committee consisting of Professor Alex Fang, Professor Mathew Kuttolamadom of the Department of Engineering Technology and Industrial Distribution, and Professor Hong Liang of the Department of Material Science at Texas A&M University. The FIB-SEM and EDS equipment used to do cross-sectional sectional imaging to analyze the elemental compositions was provided by the Material Characterization Facility at Texas A&M. All apparatus used for heat treating was supplied by Dr. Fang.

All other work conducted for the thesis was completed by the student independently.

TABLE OF CONTENTS

Page

LIST OF FIGURES

Page

LIST OF TABLES

1. INTRODUCTION

Decorative coatings are of great concern for many industries that highly regard the appearance of their products, such as jewelry, watches, and mobile phones. These products' looks are held in high regard due to the appearance of these products being one of the consumers' first areas of judgment. Therefore, an analysis must be conducted on cost-effectively decorating the product. Various methods can coat the products decoratively, varying from simple paint and dyes to vapor deposition and electro-plating, depending on the type of finish the consumer want. Each method uniquely adds a layer of coating covering the substrate in a decorative manner that can also serve as a protective layer [1]. However, many more complex coating systems require high-grade machines, which can be costly, and are deposition based.

When it comes to decorative coatings on metals, there are also various ways to do so. Painting is the go-to method for decorative coating on metals, which is easy to apply and relatively cheap. However, the downside of using paint is that it can peel or chip easily over time and often needs multiple coatings. Other established methods of decorative coatings on certain metals are anodizing and patinas which rely on grown oxides or additional layers to serve as the coatings. In the case of anodizing aluminum, a porous oxide layer is induced, after which dyes can be infused in the pores to display the desired color [2]. In the case of patinas, metallic elements such as copper and bronze chemically react with various elements of the air over time, creating a coating on the surface and causing a specific color to display [3]. The downside of using either

anodizing or patinas as a decorative coating method is that they primarily only apply to a few types of metals. However, for nearly all reflective metals, the simple use of heat and time can also be used to create an extensive range of colors [1, 4-11]. Therefore, this research explores the heat-induced color formation abilities of electrodeless nickel-plated samples and pure nickel. In addition, this research will look into the causation and theory behind the colors seen in heated nickel and factors that can affect this color formation in electroless nickel-plated samples, such as the substrate and the phosphorous content of the nickel-plated samples. The results of this research only explore the decorative capabilities and have listed the coating capabilities as future research.

1.1. Motivation

The reason for using nickel and electroless nickel-plated material stems from previous work involving heat treatment of electroless nickel-plated diamond particles. In this work, diamond particles were electroless nickel plated with different recipes for producing different phosphorous levels within the nickel coating for diamond wire saw application. After electroless nickel plating, the diamond particles were placed in their glass tube per recipe. Some particle-filled glass tubes were placed in a glove box under a vacuum, after which they were packed with argon, while others were left in an air environment. All tubes were then sealed with a cap layered with polyimide and subjected to a heat treatment at 400C for 1 hour in a kiln to crystallize the plated nickel. The initial color of the particles before heat treating was a bright silvery white, as is with most electroless nickel-plated materials. However, upon retrieving the samples from the

kiln, some samples displayed vivid colors, as shown in Figure 1, ranging from blue, reddish brown, brown, and violet. Note that the colors were uniform and of high intensity. At the time, it was unknown what caused the color formation, and it was hypothesized that the formation of an oxide layer had caused the color formation. However, it was not certain since the argon-packed samples also displayed some color, which is not supposed to happen since heat treating in an argon environment prohibits oxide formation. It was also hypothesized that there could be a correlation between the color formation and the phosphorus content within the nickel coating. As a result, further research was required due to the uncertainty of the color formation. The study involved finding out what causes such colors and whether the color can be controlled to display the desired color. Ultimately, suppose a product is electroless nickel plated and can withstand the heat and time needed to form these colors. In that case, there is the possibility for commercialization as a novel decorative coating once control of these color formations and the coating's surface characteristics are understood.

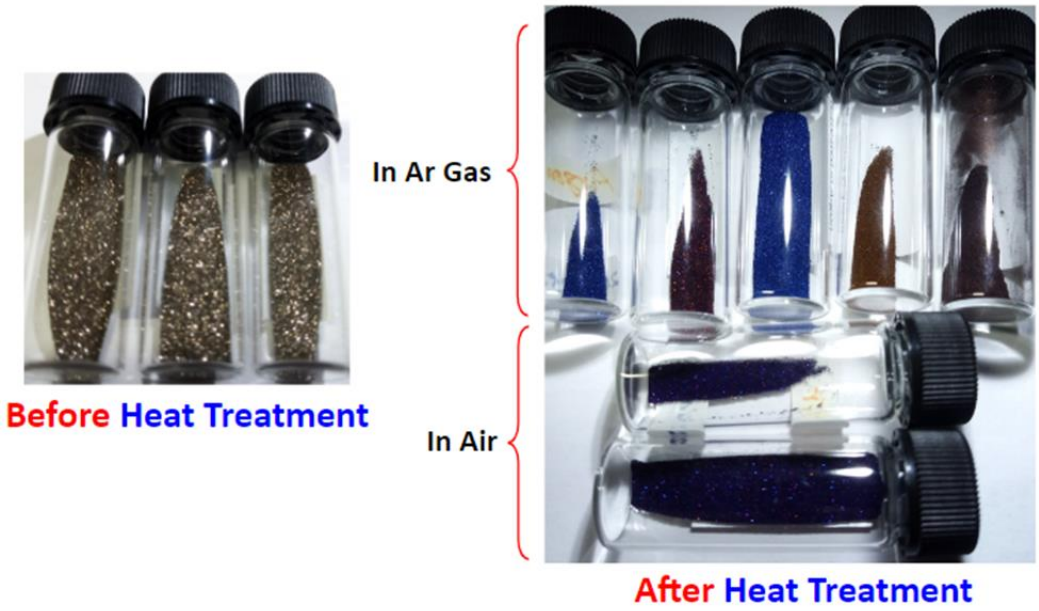

Figure 1. Before and after heat-treating nickel-plated diamond particles

1.2. Research Objectives

Due to the limited background knowledge of this research, various experiments were conducted with multiple material sizes and shapes, all consisting of either pure nickel or electroless nickel-plated substrates. The study's main goal was to understand why color formed on nickel with literature review and experimental proof and the factors affecting color formation with electroless nickel-plated samples, including phosphorous content, temperature, and time. The following research objectives were established to understand the heat-induced color formation for this research.

1. Finding the cause of colors in heated nickel
    a. Finding a method or methods to measure the hypothesized oxide layer thickness
    b. Determine the oxide layer thickness for the colored sample

2. Determining a temperature and time correlation to color formation
3. Analyzing the effect of substrate and phosphorous content on color formation

2. BACKGROUND AND LITERATURE REVIEW

2.1. Previous Research

After a thorough literature review, it has become apparent that the colors formed on metal when heated are well established. Depending on the type of metal, the name of the color formation can be called temper colors, structural colors, heat tints, or interference colors [1, 4-17]. The heat-induced colors cause a thin oxide layer altering the way light interacts, hence displaying a specific color. As a result, no physical color is formed but only light interaction, which is explained in a later section. Blacksmiths, for many years, used these colors to measure what temperature their steel piece reached during tempering hence the name temper colors [4]

Early research regarding heat-induced color on metal looked to establish the theory that the colors were caused by interference [4, 5]. During this time, efforts were also made to understand this color formation for various heated metals regarding the time and temperature required to form certain colors [4-6, 12]. However, since pure nickel is not commonly used in bulk, the focus was on other materials such as steel, stainless steel, and copper.

Later, research moved away from using heat and shifted their focus to electrochemical reactions to grow the oxide layer. A popular choice of metal was titanium since it was the easiest to control the color formations with it via electrochemical oxidation or anodization [13, 14]. Research showed how altering the

voltage during this electrochemical reaction easily controlled the color formed on the metal surface.

However, the use of heat had not completely gone away as a method to producing interference colors, only the forms in which the heat was provided. Recent research has looked into lasers as a mode to induce an oxide layer for interference colors by altering the power of the laser [16, 17]. This would allow for more precision in the location of the interference colors.

As for pure nickel, recent research focuses on oxidation kinetics, usually at high temperatures and in full oxygen environments [18-22]. During these experiments, only the mention of interference colors is provided. Also, in recent research, the focus has shifted to the deposition of either nickel or nickel oxide on various substrates [22-25]. Heat treatment afterward was conducted once again to understand oxidation kinetics or optical properties

As for electroless nickel plating research, the main focus is on oxidation behavior and optical properties, with only a mention of interference colors if developed [26-31]. This is because heat treating of electroless nickel coating is done in an argon environment to preserve the shiny silver-white color of the plating. Further research also focused on the surface properties of heat treat electroless nickel plating; however, heat-treating was conducted in an argon environment to prohibit the formation of an oxide layer [32].

Only a few articles researched color formation on nickel thoroughly [6, 10]. These articles set the basis for some of the experiments conducted in this study.

However, in general, there is a lack of research regarding the control of heat-induced color formation in nickel and electroless nickel-plated material. As a result, much of this research is exploratory and will need further study.

2.2. Thin Film Interference

As noted before, the colors formed during the heating of metals are caused by the formation of a thin oxide layer. This thin oxide layer on top of a reflective substrate causes thin-film interference, the accepted theory since the 1920s, implied when discussing colors formed on oxidized metal [4, 5]. Thin film interference is the constructive or destructive interference of light waves as they are manipulated as the light travels through a thin film and back out to the surface. Thin film interference is also the cause of color formation seen in bubbles and oil slicks on top of water [9, 11]. For clarity of how thin-film interference works, the air will be considered layer 1; the thin film will be regarded as layer two, and the area under the thin film with be considered layer three. The principle of thin-film interference goes by the following. Incident light travels across the air, layer one, and hits the surface of the thin film, layer two. As a result, some light will be reflected from the surface of the thin film, and some light will be transmitted into the thin film. The light transmitted into the thin film travels until it meets the interface of the thin film and the area beneath the thin film or layer three. Another instance of reflection and transmission occurs at the interface between layer two and layer three. The reflected light at this interface travels back up through the thin film and creates reflection and transmission at the interface between layer two and layer one.

However, it is established that the reflection at this point and all other light interactions after this point are moot since the energy of the light has decayed significantly to cause any significant change to light interference. The transmitted light from the interface between layer two and layer one then interferes with the initial reflection of the incident light at the interface between layer one and layer two. If the waves are in phase, there is constructive interference; if the waves are 180-degree out of phase, there is destructive interference. The explanation is depicted in Figure 2.

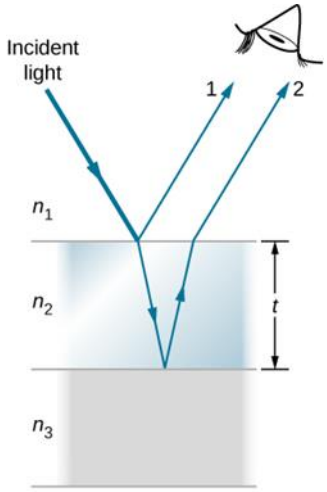

Figure 2. Model of Thin Film Interference.
Reprinted from [11]

The following two equations can be derived based on how light waves interacts during thin-film interference. Equation 1 shows when light constructively interferes, and equation 2 shows when light destructively interferes. In these equations, t is the thickness of the thin film, λ is the wavelength of light in air, n_2 is the index of refraction for the thin film, and, since colors can repeat, m is the order of the interference.

$$2t = \left(m + \frac{1}{2}\right)\frac{\lambda}{n_2} \qquad m = 0, 1, 2, 3, \ldots \textit{Destructive} \tag{1}$$

$$2t = m\left(\frac{\lambda}{n_2}\right) \qquad m = 0, 1, 2, 3, \ldots \textit{Constructive} \tag{2}$$

Note that these equations assume a monochromatic light source with a singular index of refraction for each layer, and none or both reflection points have a 180-degree phase shift. To determine if there is a 180-degree phase shift at a reflection point, the index of refraction from the layer above the reflection point must be smaller than the index of refraction from below the reflection point. Because there are only two reflection points in thin film interference scenarios if only one reflection point has a 180-degree phase shift and the other does not, then the equations for constructive and destructive interference flip. Equation 1 would become constructive interference, and Equation 2 would become destructive interference. In the case of air, nickel oxide, and nickel tri-layered system established for this research, the index of refractions is 1, 2.18, and 1.96, respectively [25, 33]. Since n1 < n2 > n3, there is only one reflection point with a 180-degree shift, the equation for destructive and constructive interference flip is shown in the equations below. The resulting thickness needed to display specific colors is given in Table 1 using MATLAB for m = 0 and m = 1 between the visible wavelengths of 400 nm to 700 nm.

$$2t = \left(m + \frac{1}{2}\right)\frac{\lambda}{n_2} \qquad m = 0, 1, 2, 3, \ldots \textit{Constructive} \tag{1}$$

$$2t = m\left(\frac{\lambda}{n_2}\right) \qquad m = 0, 1, 2, 3, \ldots \textit{Destructive} \tag{2}$$

Table 1. Thickness values for constructive and destructive interference for wavelengths between 400 and 700 nm

	Thickness (nm)			
	m = 0		m = 1	
Wavelength (nm)	Const.	Dest.	Const.	Dest.
400	45.87	0.00	137.61	91.74
450	51.61	0.00	154.82	103.21
500	57.34	0.00	172.02	114.68
550	63.07	0.00	189.22	126.15
600	68.81	0.00	206.42	137.61
650	74.54	0.00	223.62	149.08
700	80.28	0.00	240.83	160.55

It is well-established that heating metals in an oxygenated environment create various displays of colors due to thin film interference between the oxide layer and metallic backing. However, there are two requirements for oxidized metals to produce these colors: a lossy reflective metallic layer and a low-loss and low-absorbing transparent dielectric at visible wavelengths [9]. The metallic layer must be reflective to reflect as much of the incident light passed through the oxide layer back out to the surface, and it must be lossy to render moot the light transmitted into the metallic layer. The oxide layer must be transparent to allow as much incident light possible through its surface. It must be low-loss and low-absorbing so the wavelength is not entirely attenuated within the oxide layer, prohibiting interference.

2.3. Electroless Nickel Plating

Electroless nickel plating is the reduction of metal ions only at the surface of a catalytic substrate immersed into an aqueous solution of said metal ions. After an angstrom thick layer is deposited, continued deposition onto the substrate continues through the catalytic action of the deposit. This makes it a self-catalytic process at this point, in which the deposited layer catalyzes the reduction reaction until metal ions are exhausted [29, 30]. This process does not require the passage of external current, allowing it to be electroless. The method of reducing nickel metal source in water is summarized in the following chemical formula shown in Figure 3.

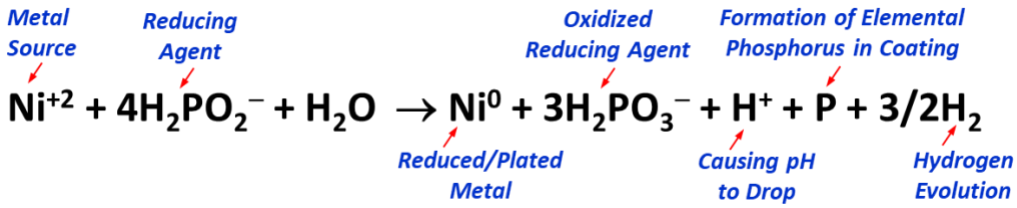

Figure 3. Chemical formula nickel metal source and reducing agent reacting in water

As noted in the chemical formula, the formation of phosphorous leads to a nickel phosphorous alloy depositing within the plated layer. Because of the phosphorous, this coating can be labeled as a nickel-phosphorous (Ni-P) coating. This phosphorous content dramatically affects the corrosion resistance of the nickel-plated layer—the more phosphorous content, the greater the corrosion resistance [29]. The amount of phosphorous in the coating is used to categorize the coating as high P, medium P, and low P. Different articles have different limits on what is considered high, medium, and low phosphorous content. For This research Ni-P Coating with High P Content (≥ 10%),

Ni-P Coating with Medium P Content (≈7%), and Ni-P Coating with Low P Content (≤ 4%).

The four essential ingredients for electroless nickel plating are the metal source, reducing agent, chelating agent, and pH adjuster. Some chemicals for each ingredient are listed in Figure 4. As noted by the chemical formula in Figure 4, the metal source of nickel is reduced by the reducing agent to create the nickel metal deposited onto the surface of the substrate. However, this chemical reaction must be controlled with a chelating agent. The chelating agent keeps the electroless nickel bath from overreacting and decomposing and regulates the reactions preventing unwanted reactions with the metal source and allowing optimal plating efficiency [30]. Finally, the pH adjuster regulates the bath's pH value, which controls the plated layer's resulting phosphorous content. A higher pH value typically results in lower phosphorus content within the coating.

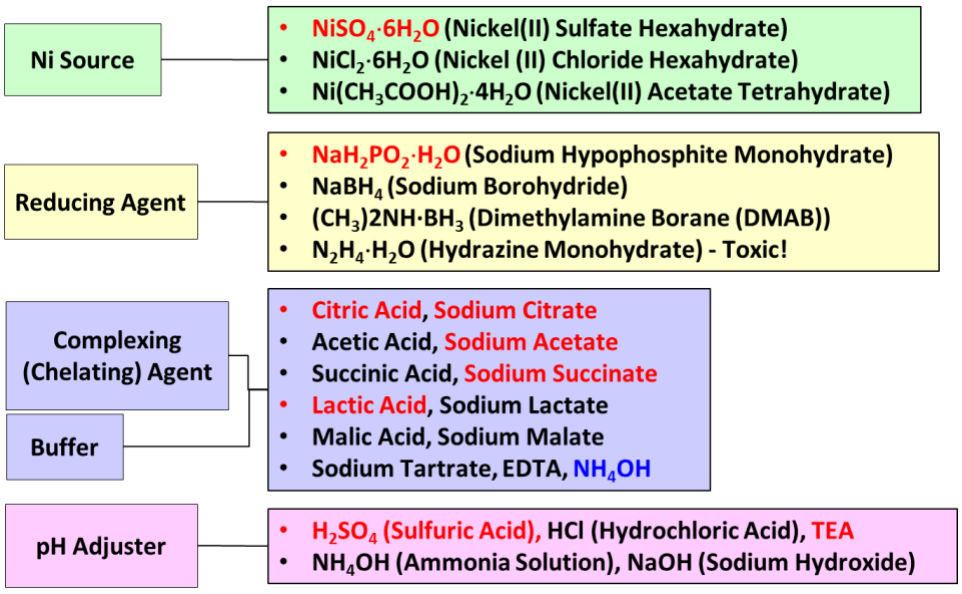

Figure 4. List of chemicals for electroless nickel plating

When comparing electroless nickel plating with electro nickel plating, we see an immediate distinction in the name alone. Electro-plating requires current, while electroless nickel plating does not. Since the current is not necessary for electroless nickel plating, conductive and non-conductive materials can be plated. The advantage of having the ability to plate any material adds to this research's potential commercialization. Electroless plating also distributes the plated layer more evenly for complex shapes than electro-nickel plating. Other differences between electro and electroless nickel plating are shown in Figure 5.

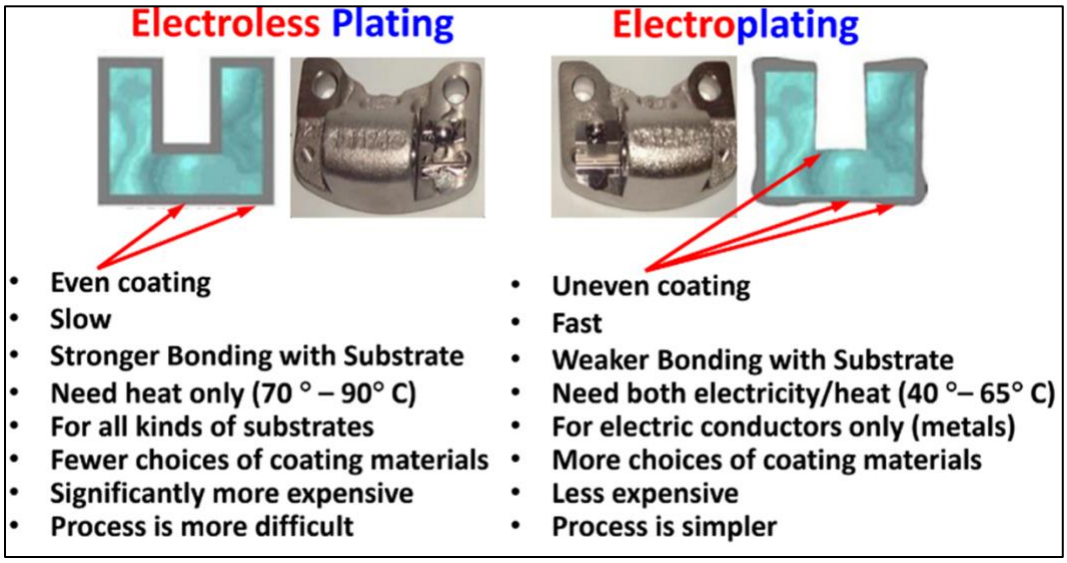

Figure 5. Difference between electroless and elector-nickel plating

As noted in the introduction, it is standard to heat-treat the electroless nickel-plated material to a temperature of 400℃ for roughly 1 hour to crystalize the grain structure since the initial deposition is amorphous. This heat treatment of the nickel-

plated material dramatically affects the surface properties of the nickel coating by increasing hardness and wear resistance [29, 30].

3. MATERIALS AND METHODS

As stated before, due to the exploratory nature of this research, various experiments were conducted on multiple types of materials consisting of either pure nickel or electroless nickel-plated materials. Therefore, this section will only list the materials and methods used for analysis. The following chapter will discuss the design of the experiments.

3.1. Nickle Plated Diamond Particles

Like the same materials used for the motivation of this research, diamond particles of mesh size 140/170 or roughly 100 μm were electroless nickel plated with nickel-phosphorous or nickel-cobalt-phosphorus. These samples were used to recreate the colors seen in the motivational section of this research. For the Ni-P samples, 12 sets of samples were coated with the same recipes that varied in pH levels, causing various expected phosphorous contents. Two samples of the 12 Ni-P plated particles were plated with different recipes that produced low and high phosphorous contents. Six samples were plated at the same pH level of 10 for the Ni-Co-P samples but varied in the Ni to Co ratio. All the samples were placed into their glass tubes for testing. The following Table 2 depicts all the nickel-plated diamond particle samples. Table 2 also lists nickel strips which are covered in the next section.

Table 2. List of electroless nickel-plated diamond particles and pure nickel strips.

Ni-P Coated Diamond		
Sample S/N	Experiment ID	Remark
A1	20140213-2	pH=6.65
A2	20140206-1	pH=6.17
A3	20140214-2	pH=6.30
A4	20140204-2	pH=6.03
A5	20140130-1	pH=5.72
A6	20140102-2	pH=5.76
A7	20140207-1	pH=6.17
A8	20131220-2	pH=5.16
A9	20140203-1	pH=5.89
A10	20140213-1	pH=6.17
2	n/a	Low P
10	n/a	High P

Ni-Co-P Coated Diamond		
Sample S/N	Experiment ID	Remark
B1 (2ea)	20170318-2	Ni:Co=1:4, pH=10
B2 (2ea)	20170318-4	Ni:Co=1:1, pH=10
B3 (2ea)	20170318-6	Ni:Co=4:1, pH=10

Ni Strips	
Sample S/N	Remark
C1 (2ea)	

3.2. Pure Nickle and Nickle Plated Strips

Aside from nickel-plated diamond particles, pure nickel strips and nickel-plated strips on different metallic substrates were also analyzed. The pure nickel strips (99.6% Ni) of size 0.2x8x100 mm were purchased on Amazon and used as a control. If the experiment called for it, the nickel strip was trimmed to size, which was the case of the nickel strips shown in Table 2. As for the nickel-plated material, three metallic substrates were used: steel, copper, and nickel labeled as Ni, Cu, and Fe, respectively. The material for the substrates was chosen due to their ease of nickel plating. Two sets of each substrate were plated. One set was coated with a high phosphorous (HP) content and the other set with a low phosphorous (LP) content. All nickel-plated strips were plated

halfway with the other half left un-plated, as shown in Figure 6. Electro nickel-plated steel strips labeled as Fe, seen in Figure 7, roughly the same size as the pure nickel strips, were also used in another experiment to understand the effect of the substrate on color formation.

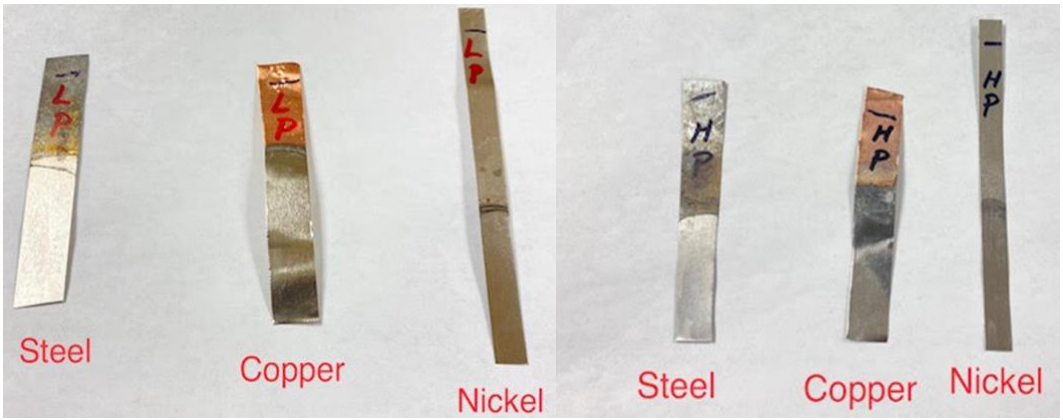

Figure 6. Half nickel-plated steel, copper, and nickel strips before heat treatment

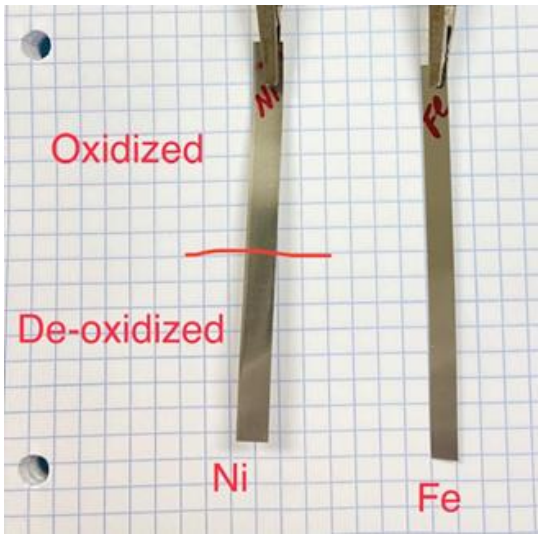

Figure 7. Pure nickel strip half deoxidized and electro nickel-plate steel strip before heat treatment

3.3. Pure Nickle Cube

For measurement of the oxide layer, pure nickel cubes (99.95% Ni) of 10 mm length were purchased from AliExpress. These nickel cubes were mirror polished by the manufacturer. Figure 8 shows the image of one of the nickel cubes.

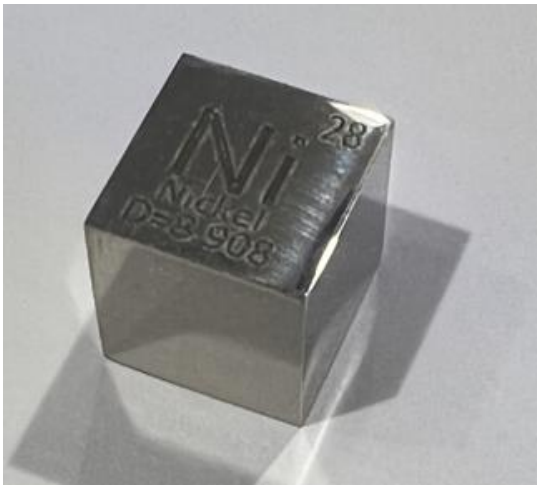

Figure 8. Mirror polished pure nickel cube before heat treatment

3.4. Nickle Plated Squares

The samples used to determine if the phosphorous content affected the color formation consisted of pure nickel squares, shown in Figure 9, which were electroless nickel plated with five different recipes. Each recipe produced an expected high, medium, or low phosphorous content, as shown in Table 3. First, the pure nickel squares were sheared from a pure nickel plate into sizes roughly 1 inch x 1 inch x 0.04 inch. Then, they were grouped accordingly and plated. Next, all extra pure nickel squares were quartered and nickel-plated with the same five recipes to measure the phosphorous content. Holes were drilled in the corner of each square for ease of plating, as shown in Figure 10.

Figure 9. Pure nickel square

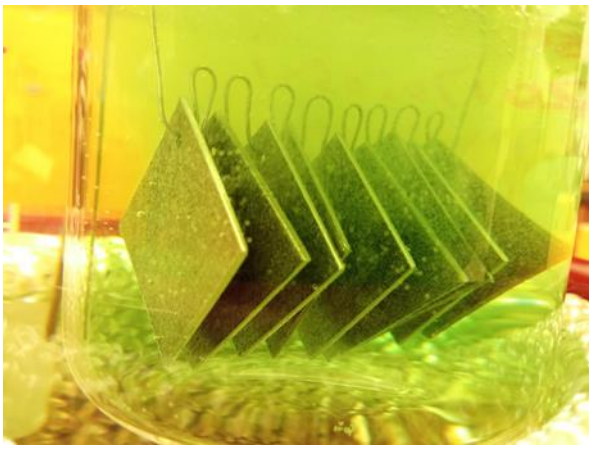

Figure 10. Pure nickel square during nickel plating

Table 3. Each nickel-plating recipe and expected phosphorous content

Recipe No.	Bath Composition/Concentration		Phosphorus Content: Expected	Original Recipie ID
1	Nickel Sulfate ($NiSO_4 \cdot 6H_2O$)	10 g/L	Low	20140207-1
	Sodium Hypophosphite ($NaH_2PO_2 \cdot H_2O$)	10 g/L		
	Sodium Succinate	5.3 g/L		
	Lactic Acid	9.3 g/L		
	pH	6.17		
	Temperature	70 °C		
2	Nickel Sulfate ($NiSO_4 \cdot 6H_2O$)	10 g/L	High	20140516-1
	Sodium Hypophosphite ($NaH_2PO_2 \cdot H_2O$)	5 g/L		
	Sodium Succinate	5 g/L		
	Sodium Citrate	5 g/L		
	pH	6		
	Temperature	70 ° C		
3	Nickel Sulfate ($NiSO_4 \cdot 6H_2O$)	10 g/L	Medium	20140522
	Sodium Hypophosphite ($NaH_2PO_2 \cdot H_2O$)	3 g/L		
	Sodium Succinate	5 g/L		
	Sodium Citrate	5 g/L		
	pH	6		
	Temperature	70 °C		
4	Nickel Sulfate ($NiSO_4 \cdot 6H_2O$)	25 g/L	High	20150104
	Sodium Hypophosphite ($NaH_2PO_2 \cdot H_2O$)	25 g/L		
	Sodium Acetate	13.6 g/L		
	Lactic Acid	2 g/L		
	Citric Acid	5.8 g/L		
	pH	4		
	Temperature	70 °C		
5	Nickel Sulfate ($NiSO_4 \cdot 6H_2O$)	20 g/L	High	20170505-1
	Sodium Hypophosphite ($NaH_2PO_2 \cdot H_2O$)	20 g/L		
	Succinic Acid	26.6 g/L		
	pH	4		
	Temperature	70 °C		

3.5. Heating Apparatuses

Three heating apparatuses were used over the various experiment depending on the availability and what the literature search had shown worked others. The first heating apparatus used was an Olympic Electric Kiln with a Bartlett V6-CF temperature controller, shown in Figure 11. This kiln was used in the first couple of experiments, with the samples hung from the top or placed on a metallic tray.

Figure 11. Olympic kiln

Due to the literature search and the uncertainty of even heating within the kiln, a SUNAVO Hot Plate (HP-102-D2) connected to an MYPIN TA4 temperature controller, as shown in Figure 12, was also used for other experiments. The hot plate allowed free

access to see the color transformation in real-time. However, the hot plate had trouble reaching and remaining at temperatures of 400℃ or above. Therefore, one last heating apparatus was used.

Figure 12. SUNAVO hot plate

The last heating apparatus used was a Zhengzhou Brother Quartz Tube Furnace (XD-12000NT), as shown in Figure 13. The experiments with this furnace ran with an open tube to allow the air environment to influence the color formation. All samples were placed on ceramic boats, as seen in Figure 14, during all heat processes.

Figure 13. Quartz tube furnace

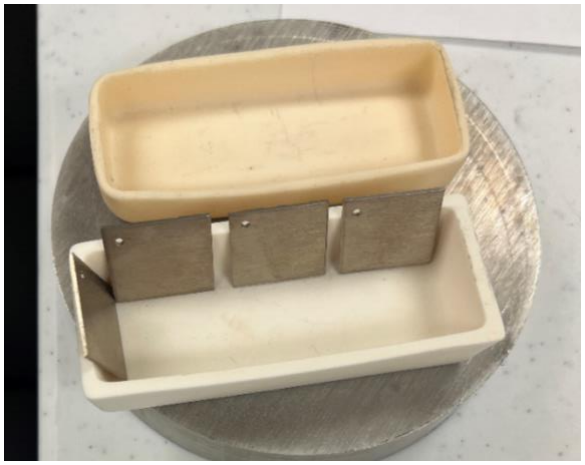

Figure 14. Ceramic boat for quartz tube furnace

3.6. Visual Observational Analysis

All experiments involved observational analysis in determining the color formed after a certain period of heating the samples. Aside from only visualizing the colors

created on the samples, pictures were taken with an iPhone 13 to display these color formations. All images for observation analysis were taken at the best visual angle in which the light minimally distorted the view during capture.

3.7. Color Measurement

Since color formation is essential for this research, a way to measure that color was implemented into one of the experiments to give the RGB values. The color sensor used was a NIX Mini2 Color sensor, shown in Figure 15. To measure the color appropriately with the color sensor, the area of analysis must fully cover its opening and lay flat

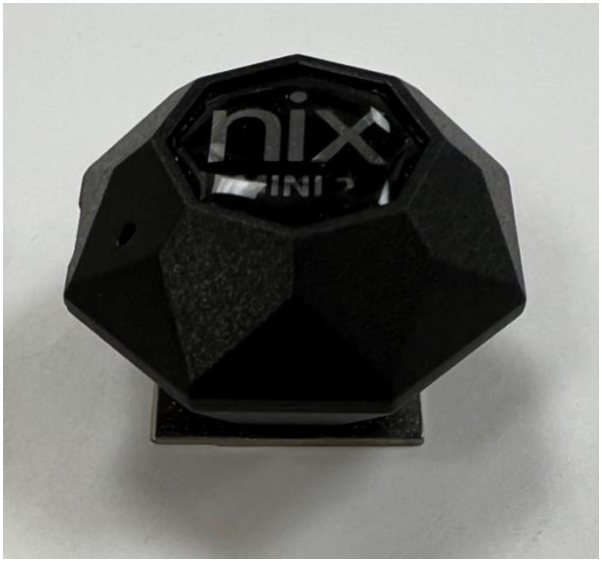

Figure 15. NIX color sensor

3.8. Ellipsometry

Ellipsometry measures the change reflected polarized light of a surface and is used to measure thin films indirectly [34]]. The requirement for optimal data collection is that the sample is as smooth as possible, very flat, and reflective so as not to scatter or

absorb the incident beam. The way ellipsometry works is monochromatic incident light is polarized and directed toward a surface. The incident light and reflected light create a plane of incidence (POI). Within the POI, there is p-polarized light which is the light electric vector parallel to the POI, and s-polarized light, which is the light electric vector perpendicular to the POI. After the reflection of a surface and into the detector, the change in polarization is formulated as the complex reflectivity ratio of p and s polarized light shown in the equation below.

$$\rho = \frac{R_p}{R_s} = \tan(\Psi) e^{i \cdot \Delta} \tag{3}$$

From this formula, the results are reported as phi (Ψ) and delta (Δ) parameters in which tan(Ψ) is the magnitude of reflectivity ratio and Δ is the phase difference between p and s reflected light. Note that the ellipsometry result alone does not give the measurement of a thin film and needs an optical model to compare the data of phi and delta. The optical model chosen for this research analysis was the Lorentz optical model used in previous research to measure oxides, and it visually fits the best [10]. The ellipsometer utilized to measure the oxide layers was a Nanofilm EP3-SE Imaging Ellipsometer (341-G), as shown in Figure 16, and was measured between 300 nm and 800 nm wavelengths at a 45-degree angle.

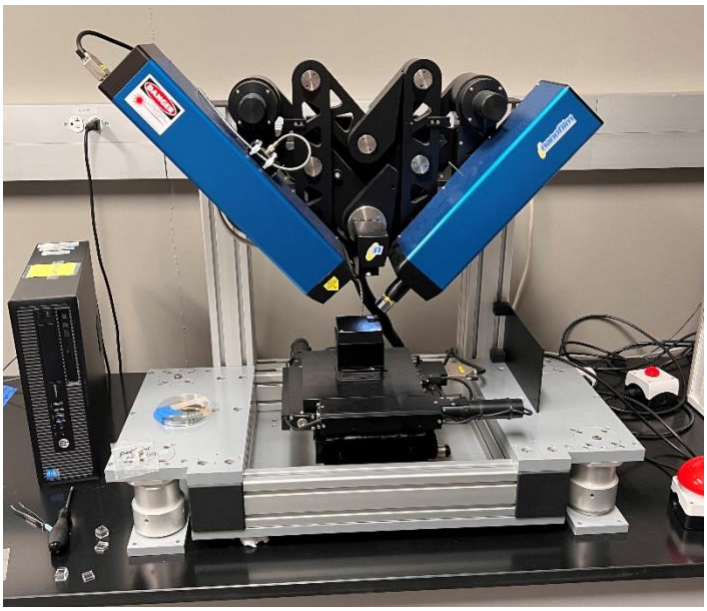

Figure 16. Imaging ellipsometer

3.9. Energy Dispersive X-Ray Analysis

Energy Dispersive X-Ray (EDS) measures the energy or an x-ray emitted when an electron of higher energy falls into a vacated space of lower energy in an atomic structure. The energy caused by the movement of electrons is unique for each element and therefore used for elemental analysis. For example, EDS was used to measure the phosphorous content of five different electroless nickel recipes after plating onto pure nickel. The EDS machine used was a JEOL JSM-7500F FE-SEM with EDS, as seen in Figure 17. All EDS analysis was completed near the center of the samples.

Figure 17. JEOL SEM with EDS

3.10. FIB-SEM Analysis

Focused Ion Beam-Scanning Electron Microscope (FIB-SEM) is used to physically see and measure the oxide layer as compared to ellipsometry which is indirect. The surface is cross-sectioned to a certain depth with the FIB and visualized with the SEM. The image of the oxide layer is then captured, and measurement is conducted with ImageJ. The FIB-SEM used was the Tescan LYRA-3 Model GMH Focused Ion Beam Microscope, as shown in Figure 18

Figure 18. Tescan FIB-SEM

4. EXPERIMENTAL DETAILS

4.1. Argon and Oxygen Heat Treatment

The basis of this experiment was to reproduce the colors that were shown as the motivation of this experiment. This test was conducted during the early stages of the literature review; therefore, it was unknown that the oxide layer was the cause of the color formation. The electroless nickel diamond particles from chapter 3.1 were used, along with a trimmed pure nickel strip from chapter 3.2. The gas-filled Ni-P samples were labeled as the Ax-series, sample 2 and sample 10. The gas-filled Ni-Co-P samples were labeled as the Bx-1 series and the Bx-2 series for the air samples. The gas-filled nickel strip samples were labeled as C1-1 and C1-2 for the air-filled nickel strip.

For the first round, argon gas was used to fill the respective nickel-plated diamond particle-filled glass tubes. Next, specific glass tubes to be filled with argon were placed in a glove box with the caps off, and a vacuum was pulled. Afterward, the vacuum was turned off, and the glove box was filled with argon. While the glove box was filled with argon, the tubes were then sealed with a metal cap layered with a thick piece of Teflon and four thin layers of polyimide (PI) to ensure the argon did not escape during the heat treatment. Once sealed, the tubes were removed from the glove box and ready for heat treatment.

The heat treatments consisted of five temperatures ranging from 200°C to 400°C in increments of 50°C and held for one hour each in the kiln from chapter 3.5. After each heat treatment, the samples were pulled from the kiln and were analyzed observationally

for any color change and pictured. At this point, no color change was expected for the argon-filled tubes since the inert gas inhibits the formation of the proposed oxide layer. The samples were not placed into the kiln until the desired temperature was reached, at which point the timer also started.

For the second round, oxygen gas was used to go along with the hypothesis that an oxide layer was the cause of the color. The process of pulling a vacuum in a glove box and filling it with oxygen was repeated with the same samples from the argon gas round. However, samples A2, A3, A4, and A5 were not packed since their lid could not be opened to allow oxygen to fill their tubes. In addition, sample A8 was not adequately packed since its lid could not tighten fully as the threads were stripped. Also, the Bx-2 series, Cx-2 series, and samples 2 and 10 were not used for the oxygen experiment since they were either used already in the air-filled portion of the experiment or had already established a distinct color.

4.2. Effect of Substrate

This test was conducted to see if the substrate of a nickel-plated sample had any effect on the color formation. The initial thought was that there would be no effect since the thin oxide film associated with the color formation only grew from the outermost layer, which was the nickel coating.

Two tests were conducted on different heating mediums; however, the goal was the same in analyzing if the substrate affected the color formation. The material used for the first test was the electroless nickel-plated Ni, Cu, and Fe strips from chapter 3.2.

First, the high phosphorous samples were heated in the kiln, hanging from the top, at 400℃ for 50 minutes and visually observed and pictured at the 20, 30, 40, and 50-minute mark. The heating of the samples went by the following. First, the samples were not placed into the kiln until the temperature reached 400℃, at which point the timer was started. Then, once the kiln door was opened for visual observation, the timer was stopped and started again once the kiln door was closed and reached back up to 400℃. Next, the process was repeated with the low-phosphorous samples.

The second test was conducted on a hot plate due to some literature findings that also used a hot plate. The material for this test was a pure nickel strip labeled as Ni and an electro nickel-plated steel strip labeled as Fe from chapter 3.2. All strips were degreased in a sodium hydroxide (NaOH 10%) for 2 minutes, DI water rinsed for 30 seconds, deoxidized with sulfuric acid (H_2SO_4 10%) for 2 minutes, and DI water rinsed for 30 seconds. However, for the pure nickel strip, only half of the strip was deoxidized, as shown in Figure 7, to see if there was a change. One pure nickel strip and one electro nickel plated steel strip were heated on the hot plate mentioned in chapter 3.5 at roughly 380℃ since the hot plate could not maintain 400℃ for 50 minutes. Every 10 minutes, the strips were visually observed and pictured. Due to the results of the electro-nickel-plated steel strip, a second steel strip was subjected to the hot plate for 5 minutes, and the color change was captured on video. The first electro-nickel-plated steel strip was cut into smaller sections and taken to the EDS for elemental analysis.

4.3. Nickel Oxide Layer Measurement

This test measured the oxide in two ways: via ellipsometry and with FIB-SEM. At this point, it was established that the oxide layer was the cause of the color formation. The material used was three pure nickel cubes from chapter 3.3. All cubes were degreased in a sodium hydroxide (NaOH 10%) for 2 minutes, DI water rinsed for 30 seconds, deoxidized with sulfuric acid (H_2SO_4 10%) for 2 minutes, and DI water rinsed for 30 seconds. Next, they were heat treated in the quartz tube furnace mentioned in chapter 3.5 at 425℃. All cubes were placed in the furnace simultaneously and removed after a specific time. Cube one was heated for 15 minutes, cube 2 for 30 minutes, and cube 3 for 50 minutes. After each cube was removed, they were air-cooled and visually observed. The ellipsometer from chapter 3.8 was then used to measure the oxide layers of each sample. Afterward, cube two was taken to the FIB-SEM for cross-sectioning and observation of the oxide layer pertaining to that color produced on the cube. The oxide layer was measured with ImageJ and compared to the ellipsometry measurement and the thin film interference calculation.

4.4. Effect Of Phosphorous Content

This test aimed to determine to what extent the phosphorus content affected the color formation on electroless nickel-plated nickel. Since the higher the phosphorous content has higher the corrosion resistance, it was expected that the higher the phosphorous content, the slower the color forms. The material used for this experiment is the electroless nickel-plated pure nickel squares from chapter 3.4, shown in Figure 19.

Each column represents the recipe number used, starting from left to right. Note the difference in reflectivity among each recipe's samples. As a control, three pure nickel squares were left un-plated. The heat treatment was conducted at three different temperatures 350℃, 400℃, and 450℃. Three-time limits of 30, 60, and 90 minutes were imposed for each temperature. For each temperature and time, five samples were used, one from each recipe totaling nine groups of five samples, and were labeled as shown in table 4. The pure nickel squares were heat treated separately and one sample per temperature and cycled the various time limits for the single temperature. After each heat treatment, the samples were air-cooled, visually observed, pictured, and color-scanned with the color sensor from chapter 3.7.

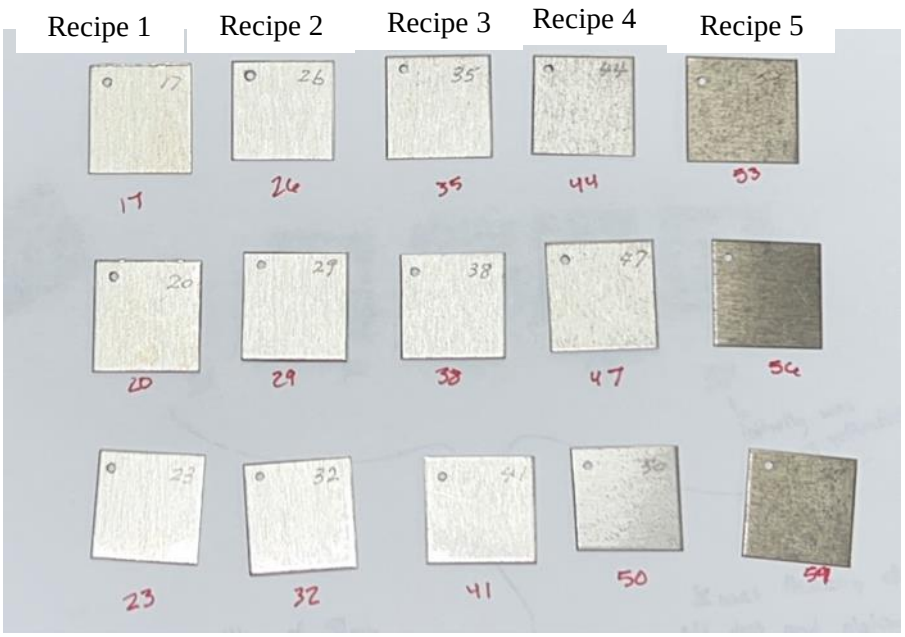

Figure 19. Nickle plated nickel squares before heat treatment

Table 4. Groups and labels for nickel-plated squares

	Group/Sample ID		
Time/Temperature	350C	400C	450C
30 min	(A) 17,26, 35, 44, 53	(B) 18, 27, 36, 45, 54	(C) 19, 28, 37, 46, 55
60 min	(D) 20, 29, 38, 47, 56	(E) 21, 30, 39, 48, 57	(F) 22, 31, 40, 49, 58
90 min	(G) 23, 32, 41, 50, 59	(H) 24, 33, 42, 51, 60	(I) 25, 34, 43, 52, 61

The quarter samples mentioned in chapter 3.4 were gathered to measure each recipe's phosphorous content. One from each recopied was mounted onto an aluminum stock shown in Figure 20, and EDS was then conducted on the mounted quartered samples

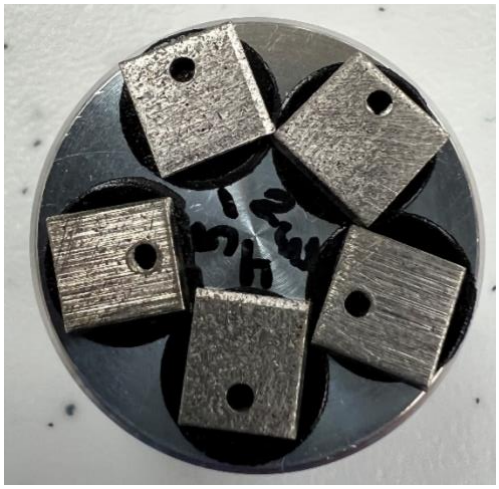

Figure 20. Mounted quartered nickel-plated nickel squares for EDS

5. RESULTS AND DISCUSSION

5.1. Argon and Oxygen Heat Treatment

As stated before, the goal of this experiment was to try and reproduce the colors visualized during the experiment that motivated the drive for this research. The first rounds of heat treatment in argon and air environment. From temperatures between 200℃ to 300℃, there was no color change in the Ax, Cx-1, Cx-2 series, sample 2, and sample 10. However, the Bx-1 and Bx-2 series darkened slightly. At 350℃, samples A8, A9, sample 2, and sample 10 produced a light straw tint. At 400℃, all the Ax, Cx-1, and Cx-2 produced a light brown tint, and the Bx-1 and Bx-2 series remained the same from 350℃. However, at 400℃, the lids of samples 2 and 10 seemed to have popped off during the heat treatment. Upon inspection, samples 2 and 10 both produced distinct colors of brown and dark purple, respectively, shown in Figure 21. The production of colors in samples 2 and 10 after heat treatment at 400℃ with their lids off hinted that both the sealed argon and air-filled samples did not allow a formation of a large enough oxide layer due to lack of or inadequate amount of oxygen to react with the nickel plating.

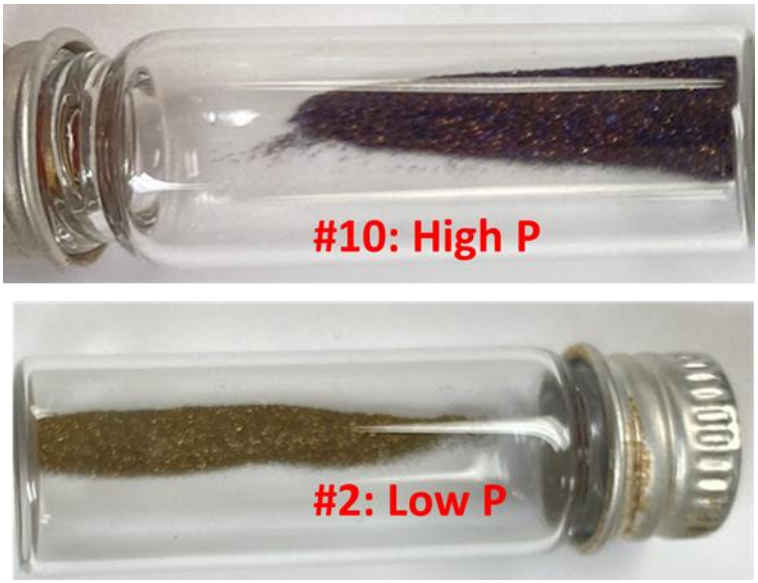

Figure 21. Sample 2 and 10 after 400℃ for 1 hour

The second round involved recycling the same samples from the argon round except for the samples discussed in chapter 4.1. This time, since the hypothesis was that the colors were due to the oxide layer, the samples were packed with oxygen. Between 200℃ and 300℃, there was no change in color than the light brown tint of the argon round. At 350℃, there was further light brown tinting on the Ax and Cx-1 series. At 400℃ samples, A3 and A7 produced a darkened purple tone, while all the other Ax and Cx-1 series produced a brown-gold color, as shown in Figure 22. The Bx-1 series had no color change. The defined brown coloring in the oxygen environment proved that further oxidation was induced. However, since it was limited by the amount sealed into the tube, further oxidation could not be achieved compared to samples 2 and 10, whose caps were off, allowing unlimited oxygen in the air.

Figure 22. Nickel-plated diamond particle in oxygen after 400°C for 1 hour

5.2. Substrate Effect

This experiment aimed to understand if the substrates affected color formation. The first test conducted in the kiln with the high phosphorous samples showed the following. At 20 minutes, Ni, Cu, and Fe all produced a brown color which darkened at the 30-minute mark for Ni and had hints of red for the Cu and Fe samples. At 40 minutes, the Ni sample remained brown, while the Cu and Fe samples began to produce some hints of purple in their reddish-brown overtone. Finally, at 50 minutes, the Ni sample formed some reddish-brown tones while the pule color grew in the Cu and Fe samples. The next test conducted in the kiln with the low phosphorous showed the following. At 20 and 30 minutes, Ni and Cu showed some straw tinting, and Fe showed some brown coloring with darker tones near the top of the plated section. The 40-minute mark produced no change; however, at 50 minutes, Ni and Cu got slightly darker in their

straw tone, and Fe started to make brown-reddish color with some dark purple forming near the center. The samples after the total heat treatment can be seen in Figure 23. From this result, we can see that for both the high and low phosphorous samples, the Fe substrate produced the most variation in color, and more so with the high phosphorous content.

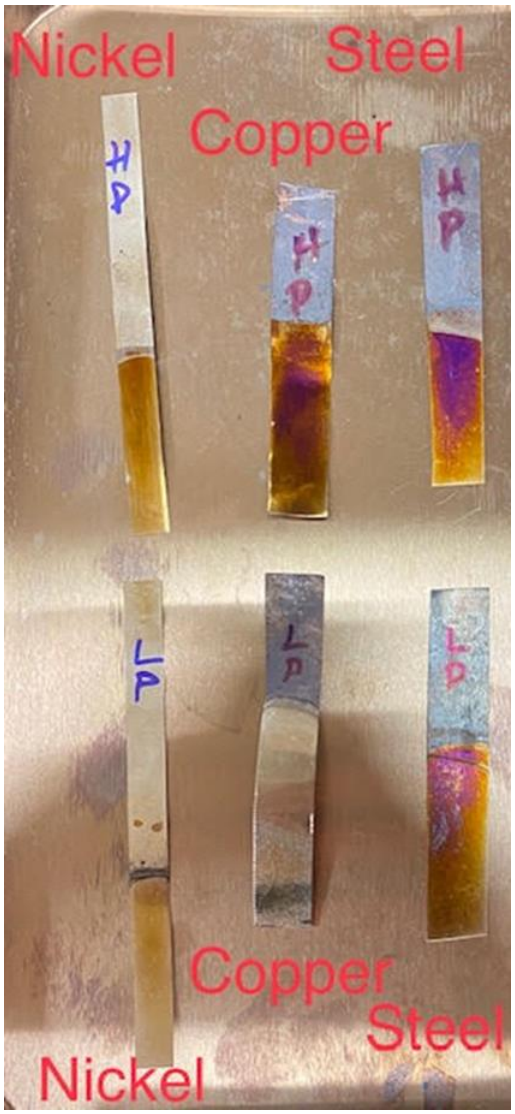

Figure 23. Nickle plated steel, copper, and nickel substrates after heating at 400°C for 50 minutes

The second test was conducted in the hot plate and showed the following. For 50 minutes, the pure Ni sample obtained a light straw tint. As for the electro-nickel-plated Fe strip, within the first 10 minutes, it went through a light straw color, brown, reddish brown, purple, blue, and light blue. For the remainder of the time, the Fe strip got lighter blue to the point where straw and brown started to take over the sample again at the 50-

minute mark, as shown in Figure 24. This sample was saved for EDS analysis. Due to the Fe sample's rapid color, a second Fe sample was heated for only five minutes until a dark purple and dark blue covered the entire strip. This process was videotaped to reveal the order of colors that form. Within these five minutes, the color order went from light straw to brown to reddish brown to dark red, to dark purple, then blue. After this point, the blue lightens and reveals straw once again.

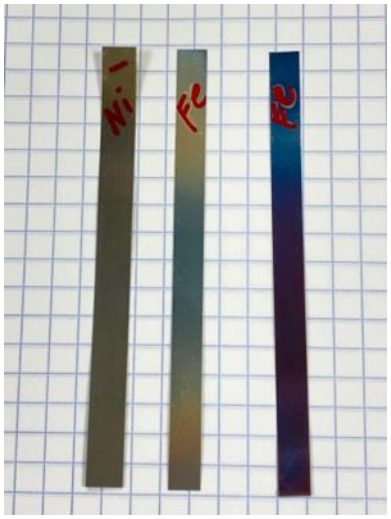

Figure 24. Pure nickel strip and both electro nickel plated steel strips after heat treating

The first EDS analysis was an area scan showing the spectrum of elements present, as shown in Figure 25. The elemental weight percentages are displayed in Table 5. The EDS scan showed a high weight % of oxygen and nickel, as expected; however, there is also a significant weight % of iron and carbon, which indicates that during the heat treatment, there was possibly diffusion of the steel elements past the nickel plating

also being oxidized at the high temperature. Since steel oxidizes faster than nickel, the variation of the color showed up more quickly due to oxidized steel elements.

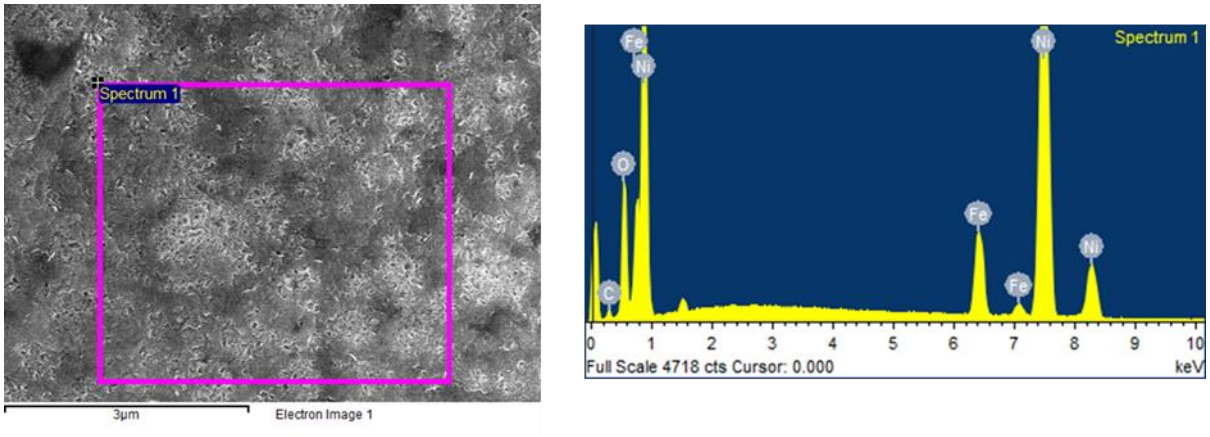

Figure 25. EDS elemental analysis of the scanned area

Table 5. Atomic % and weight % of elements present in the EDS scanned area

Element	Weight%	Atomic%
°C K	3.34	11.12
O K	12.45	31.16
Fe K	8.64	6.20
Ni K	75.57	51.53
Totals	100.00	

A second EDS scan showed the distribution of the four elements listed above within the areal scan, as shown in Figure 26. This scan again depicts the steel substrate's influence on the color formation, for it is spread densely over the entire scanned area.

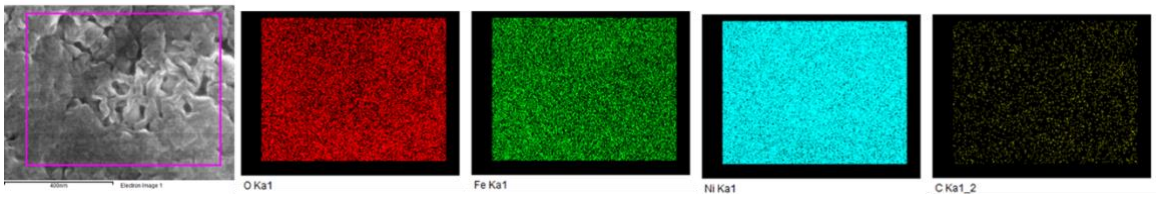

Figure 26. Elemental distribution of the EDS scanned area

However, it is also possible that the recorded high weight % can be attributed to the high energy of the electron beam penetrating significantly into the steel substrate. Therefore, further analysis should be conducted with lower beam energy to prevent the possibility of a large penetration depth. Also, EDS can be completed on an electro-nickel-plated sample that has not been oxidized to serve as a control.

5.3. Measurement Of Oxide Layer

Since the literature agrees that an oxide layer causes color formation, measuring it and comparing it against thin film interference calculations was critical. After heating the nickel cubes at 425℃ for 15, 30, and 50 minutes, the colors were light brown, reddish brown with some purple, and blue, respectively, all shown in Figure 27. Therefore, the first method used to measure the oxide layer was ellipsometry. After obtaining the phi and delta data points and fitting them against the Lorentz optical model, the measured nickel oxide thickness values were 98.1 nm, 95.6 nm, and 98.7 nm, respectively. The most obvious discrepancy is that the oxide thickness value for cube 2 was lower than cube 3, which is impossible since the 30-minute sample should have a larger oxide thickness. This error can be attributed to the extensive root mean squared

error (RMSE) values attributed to each measurement when fitting the data to the optical model. This large RMSE is assumed to be attributed to the subpar sample surface concerning the requirements for proper measurement with an ellipsometry machine explained in chapter 3.8. Due to this significant error, a more direct approach was used to measure the oxide layer.

Figure 27. Color of heat-treated cubes at 425°C for 15, 30 and 50 minutes

The second method used was FIB-SEM. Due to the high cost of this machine, only cube two was used. Two FIB cross-sections were completed to reveal the nickel oxide layer, as shown in Figures 28 and 29. Measurement one was near the edge, and measurement two was near the center. The values measured were 53.9 nm and 53.6 nm, respectively, shown in Tables 6 and 7. When comparing it to thin film interference calculations at 400 nm wavelength and m = 1 since purple is the start of the second order in thin film interference calculation, the equation gives a thickness value of 137.61 nm, which is a 90.9% difference between the measured value and the calculated value. This significant percent difference can be because thin film interference calculations do not assume multi-chromatic light sources for which multiple wavelengths can interfere, changing the dynamic of the thin film interference calculations.

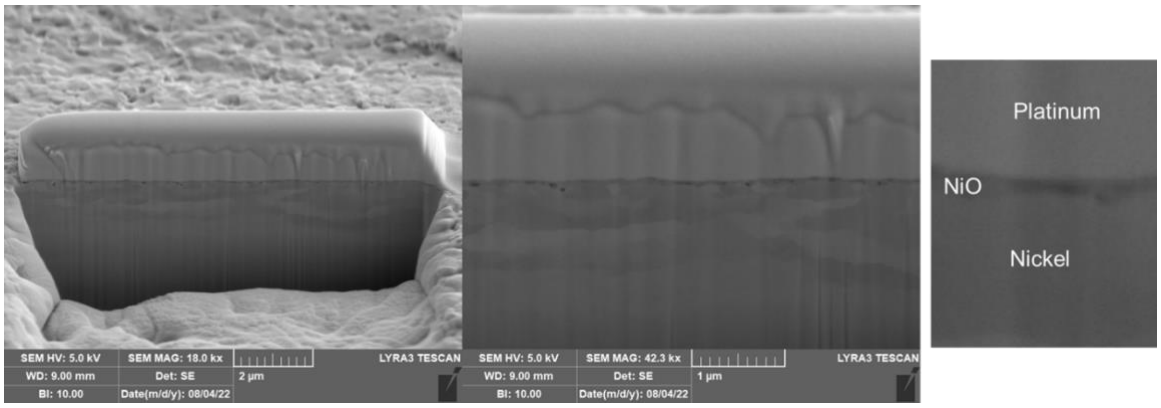

Figure 28. FIB-SEM cross section near the edge of cube two

Table 6. The average thickness of the nickel oxide layer near the edge of cube two

	Label	Length (nm)
1		51.907
2		56.144
3		59.322
4		56.409
5		50.053
6		46.875
7		57.203
8		53.496
9	Mean	53.926
10	SD	4.139
11	Min	46.875
12	Max	59.322

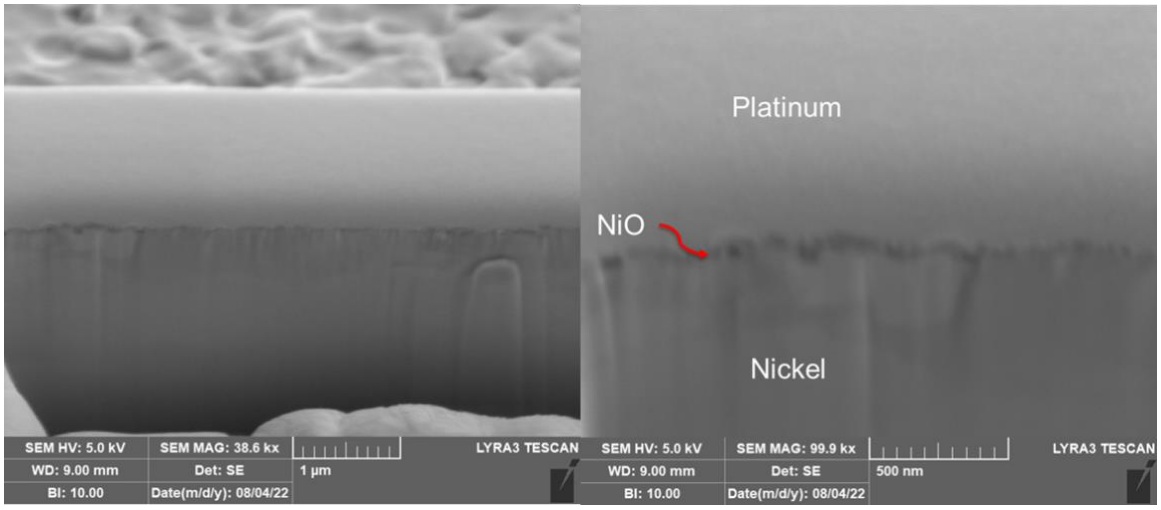

Figure 29. FIB-SEM cross section near the center of cube two

Table 7. The average thickness of the nickel oxide layer near the center of cube two

	Label	Length (nm)
1		46.622
2		53.378
3		51.351
4		47.748
5		50.45
6		58.559
7		49.55
8		55.405
9	Mean	51.633
10	SD	3.987
11	Min	46.622
12	Max	58.559

5.4. Phosphorous Content Effect

As stated in the introduction, electroless nickel plating creates a Ni-P alloy in the plated layer where the phosphorous content can be controlled. Therefore, this test was completed to see the effect of that phosphorous content on color formation.

The following phosphorous weight percentages, shown in Table 8, were obtained with EDS area analysis. For reference, each area was analyzed twice and averaged.

Table 8. Measure the phosphorous content of each nickel-plating recipe

Recipe No.	Measured P Content weight %
1	8.82%
2	8.20%
3	6.41%
4	9.38%
5	0.41%

For the first series of samples heated at 350°C, all the nickel-plated samples started with a light straw tinting at 30 minutes and darkened to a brown color during the 60 and 90-minute intervals shown in Figure 30. Also, as the color developed into a more defined brown, the color sensor could pick up on the actual color seen in person, as shown in Figure 31. The most prevalent color formation came from recipe 3, which is the most evenly distributed and already reaching some slight reddish tones. Meanwhile, the pure nickel samples remained slightly tinted with a straw color throughout the first series.

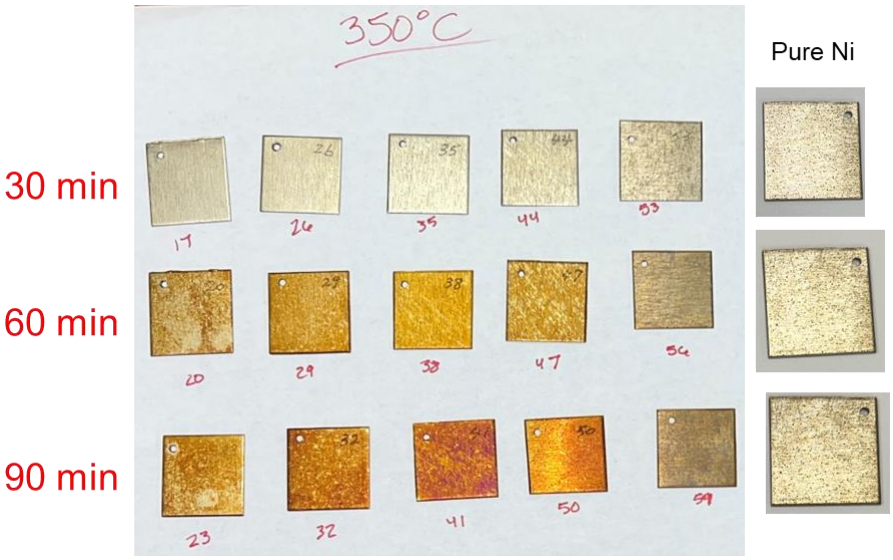

Figure 30. Heat treatment results of groups A, D, and G

Figure 31. Color scan of groups A, D, and G

For the second series conducted at 400℃, we see the nickel-plated samples start at a reddish-brown color at 30 minutes and work their way to either a blue or light blue color by the 90-minute mark in Figure 32. The color sensor picked up on these color changes in the blue phase; however, it began registering purple when the blue-toned lightened, as seen in Figure 33. Also, with recipe 5, the samples seemed to remain dark blue after the 60-minute mark, and the pure nickel samples started to gain a darkened overtone with no color change.

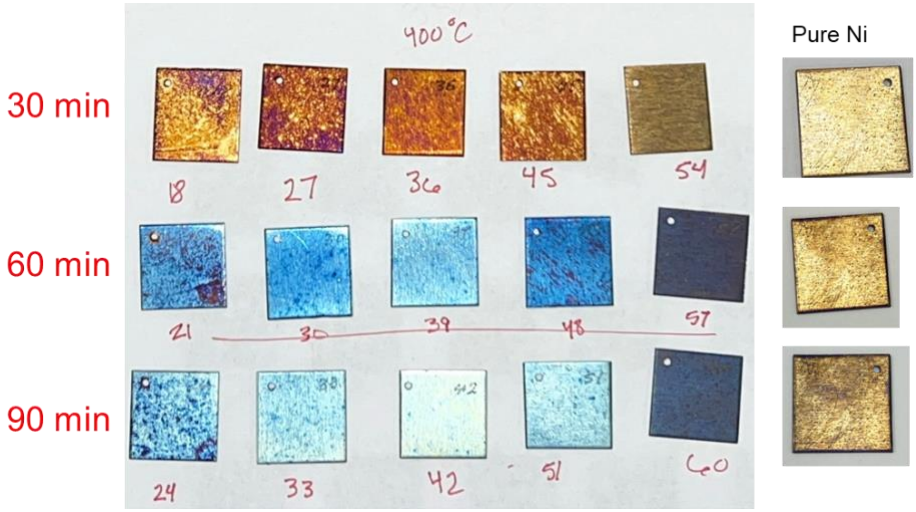

Figure 32. Heat treatment results of groups B, E, and H

Figure 33. Color scan of groups B, E, and H

For the third series done at 450°C, the nickel-plated samples start in the blue and light blue at 30 minutes and then vary significantly for each recipe afterward. At the 60-minute mark, recipes 2,3, and 4 developed a reddish-purple tone with some hints of dark blue, while recipe 1 developed chiefly a brown color with some purple, and recipe 5 lighted up to a grey-black color. At the 90-minute mark, recipes 1, 2, 4, and 5 remained the same from 60 minutes, while recipe 3 formed blue-green color not noted before in any literature, as seen in Figure 34. The color sensor recognized the colors correctly, as seen in Figure 35. As for the pure nickel sample, a slight tint of light blue with some

grey tones developed at the 30-minute mark and remained that way throughout the entire third session.

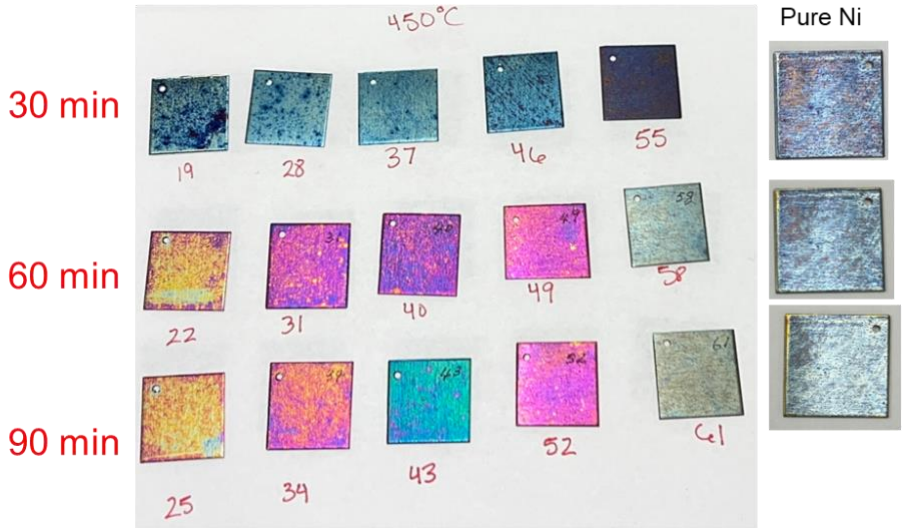

Figure 34. Heat treatment results of groups C, F, and I

Figure 35. Color scan of groups C, F, and I

From these results, we see that objectively recipe 3, with a measured phosphorous content of 6.41 weight %, produced the most significant variation in color along with a relatively even distribution of color among the entire sample. When comparing the nickel-plated samples to the pure nickel samples, except for recipe 5, all the other recipes allowed a greater variety of color formation. However, as seen from the initial look of the samples before heat treatment, there can also be a correlation between

the initial reflectivity of the sample and the color-forming ability after heat treatment. Weaker reflective samples do not produce color effectively as higher reflective samples.

6. CONCLUSIONS AND FUTURE INVESTIGATIONS

As shown from this research, multiple conclusions came to be made from the various experiments. First and foremost, through literature search and experiments regarding the measurement of the oxide layer, it has become apparent that the oxide layer is responsible for the color formation seen when heating both pure nickel and electroless nickel-plated substrates due to thin film interference. Using FIB-SEM, an image could be captured showing the oxide layer's presence and its size when the pure nickel cube was a purple color. Ellipsometry was also used to measure the oxide layer indirectly but failed to do so due to the subpar surface of the sample, which both scattered and adsorbed the incident beam, inhibiting the reflected beam's full potential to sense by the sensor for good analysis. A remedy for using ellipsometry to measure the oxide layer would be to nickel plate a glass substrate to have a smoother surface and hopefully better reflectivity after heat treatment. Further analysis is required on nickel-plated substrates that have formed a color to compare their measured oxide layer with pure nickel. Also, since ellipsometry can obtain the optical constant of a material, the optical constants of electroless nickel-plated materials can be obtained to better tune the thin film interference calculation for better control of the thickness required for specific color formation.

Following the first experiment, it can be concluded that proper sealing between the argon-filled glass tube and cap inhibits the growth of an oxide layer, preventing thin film interference in the sample. As a result, the color formed during the research that

motivated this research was due to improper sealing and more than likely allowed an air environment to being present in the diamond particles when heat treating. Also, in the first experiment, it can be concluded that the coloring of heated nickel-plated material can be achieved in a pure oxygen environment. However, due to the limited amount of oxygen sealed with the tube, it was not enough to cause a variety of colors after it was depleted. Compared to the samples whose lids came off during heat treatment and were able to develop defined colors due to the unlimited amount of oxygen in the air, the oxygen-packed samples were only able to for up to a straw color before depletion of the oxygen within the tubes. Further research is needed on heating electroless nickel-plated samples in a pure oxygen environment to see if controlling the oxygen in the environment can further control the color formation. For instance, if only some oxygen is available during heat treatment, the nickel-plated samples can only form up to this color.

Next, looking at the effect of the substrates, it can be concluded the type of metallic substrate does affect the color formation as seen with visual observation. With the EDS analysis obtained, it is possible that the nickel-plated steel substrate cycled through its color sequence faster due to diffusion of the steel elements past the nickel layer during heat treatment, allowing faster oxidation of these steel elements. It is also possible that the beam energy used for EDS analysis penetrated deep past the nickel and nickel oxide layer, contributing to the dense levels of carbon and iron in the scan. Further research is required to validate if diffusion of the substrate material is the true cause of the fast or slower color formation. Further research must be conducted on other

nickel-plated substrates that can withstand the temperature required to produce thin film interference further to validate this process as a decorative coating.

Finally, the phosphorous content experiment concluded that a medium phosphorous content produced the most significant variation in colors. It was expected that the lower phosphorous content would produce the greatest variation in color due to its lower corrosion resistance. However, the phosphorous content experiment and the substrate effect experiment showed how a medium to high phosphorous content sample produced a more significant color variation. The color variation could also be attributed to the initial reflectivity of the coating right after nickel plating, which showed that the low-phosphorous sample produced a low-reflective coating. Low reflectivity initially leads to poor thin film interference, causing the color, if any, to be dull. Aside from phosphorous content affecting the color, this experiment and others show that the best temperature to control color formation is between 400°C and 425°C. Between these temperatures, while heat treating in the air, the color forms at a steady pace, beginning at roughly the 15-minute mark with straw to light blue at approximately the 60-minute mark. Further research is needed to fine-tune the time and temperature required precisely to produce a specific color since many other variables come into play, such as the evenness of the heating and the oxygen content present.

As stated in the introduction, this research purely focuses on the decorative aspect of this coating. Therefore, future research also requires that studies are conducted on the coating aspect as well. The coating's surface properties to be studied include scratch-resistant, passive/corrosion resistance, wear-resistant, and other properties that

make up a good coating. It is essential to understand the coating surface properties since the commercialization of this process deems it necessary that the coating is not only decorative but a reliable one with other purposes besides it looking nice.

REFERENCES

[1] G. Reiners, U. Beck, and H. A. Jehn, "Decorative optical coatings," *Thin Solid Films,* vol. 253, no. 1-2, pp. 33-40, 1994.

[2] J. M. Runge, "A brief history of anodizing aluminum," *The Metallurgy of Anodizing Aluminum,* pp. 65-148, 2018.

[3] T. Graedel, "Copper patinas formed in the atmosphere—II. A qualitative assessment of mechanisms," *Corrosion Science,* vol. 27, no. 7, pp. 721-740, 1987.

[4] C. W. Mason, "Temper Colors," *The Journal of Physical Chemistry,* vol. 28, no. 12, pp. 1233-1244, 1924/12/01 1924, doi: 10.1021/j150246a001.

[5] U. R. Evans, "The colours due to thin films on metals," *Proceedings of the Royal Society of London. Series A, Containing Papers of a Mathematical and Physical Character,* vol. 107, no. 742, pp. 228-237, 1925.

[6] D. McAdam and G. Geil, "Rate of oxidation of typical nonferrous metals as determined by interference colors of oxide films," *J. Res. Natl. Bur. Stand.(1934),* vol. 28, no. 5, p. 593, 1942.

[7] K. Gupta, J. Marton, and J. Shewchun, "Oxidation Characteristics of Some Nickel Alloy Films in Air and Water Vapor," *Journal of The Electrochemical Society,* vol. 121, no. 1, p. 118, 1974.

[8] J. Łabanowski and M. Głowacka, "Heat tint colours on stainless steel and welded joints," *Welding International,* vol. 25, no. 7, pp. 509-512, 2011.

[9] M. A. Kats, R. Blanchard, S. Ramanathan, and F. Capasso, "Thin-film interference in lossy, ultra-thin layers," *Optics and Photonics News,* vol. 25, no. 1, pp. 40-47, 2014.

[10] T. Letsou, M. ElKabbash, S. Iram, M. Hinczewski, and G. Strangi, "Heat-induced perfect light absorption in thin-film metasurfaces for structural coloring," *Optical Materials Express,* vol. 9, no. 3, pp. 1386-1393, 2019.

[11] R. H. Paul Peter Urone, " Thin Film Interference," in *College Physics 2e*. Houston, Texas: OpenStax, 2022.

[12] C. Leberknight and B. Lustman, "An optical investigation of oxide films on metals," *JOSA,* vol. 29, no. 2, pp. 59-66, 1939.

[13] E. Gaul, "Coloring titanium and related metals by electrochemical oxidation," *Journal of chemical education,* vol. 70, no. 3, p. 176, 1993.

[14] M. V. Diamanti, B. Del Curto, and M. Pedeferri, "Interference colors of thin oxide layers on titanium," *Color Research & Application: Endorsed by Inter-Society Color Council, The Colour Group (Great Britain), Canadian Society for Color, Color Science Association of Japan, Dutch Society for the Study of Color, The Swedish Colour Centre Foundation, Colour Society of Australia, Centre Français de la Couleur,* vol. 33, no. 3, pp. 221-228, 2008.

[15] V. Veiko *et al.*, "Controlled oxide films formation by nanosecond laser pulses for color marking," *Optics express,* vol. 22, no. 20, pp. 24342-24347, 2014.

[16] R. Zhou, T. Huang, Y. Lu, and M. Hong, "Tunable coloring via post-thermal annealing of laser-processed metal surface," *Applied Sciences,* vol. 8, no. 10, p. 1716, 2018.

[17] X. Ma *et al.*, "Coloring stability analysis of nanosecond pulsed laser induced surface coloring on stainless steel," *Optics & Laser Technology,* vol. 123, p. 105936, 2020.

[18] E. Gulbransen and K. Andrew, "The kinetics of oxidation of high purity nickel," *Journal of the Electrochemical Society,* vol. 101, no. 3, p. 128, 1954.

[19] M. Graham and M. Cohen, "On the mechanism of low-temperature oxidation (23–450 C) of polycrystalline nickel," *Journal of the electrochemical society,* vol. 119, no. 7, p. 879, 1972.

[20] G. C. Allen, P. M. Tucker, and R. K. Wild, "Surface oxidation of nickel metal as studied by X-ray photoelectron spectroscopy," *Oxidation of Metals,* vol. 13, no. 3, pp. 223-236, 1979.

[21] J. Pivin, J. Morvan, and D. Mairey, "The influence of surface polishing on the oxidation of pure nickel," *Acta Metallurgica,* vol. 32, no. 12, pp. 2203-2212, 1984.

[22] A. López-Beltrán and A. Mendoza-Galván, "The oxidation kinetics of nickel thin films studied by spectroscopic ellipsometry," *Thin Solid Films,* vol. 503, no. 1-2, pp. 40-44, 2006.

[23] P. Mohanty, C. Rath, P. Mallick, R. Biswal, and N. Mishra, "UV–visible studies of nickel oxide thin film grown by thermal oxidation of nickel," *Physica B: Condensed Matter*, vol. 405, no. 12, pp. 2711-2714, 2010.

[24] I. Valyukh, S. Green, H. Arwin, G. A. Niklasson, E. Wäckelgård, and C.-G. Granqvist, "Spectroscopic ellipsometry characterization of electrochromic tungsten oxide and nickel oxide thin films made by sputter deposition," *Solar Energy Materials and Solar Cells*, vol. 94, no. 5, pp. 724-732, 2010.

[25] S. A. Mahmoud, A. Shereen, and A. T. Mou'ad, "Structural and optical dispersion characterisation of sprayed nickel oxide thin films," *Journal of Modern Physics*, vol. 2011, 2011.

[26] J. Marton and E. Chan, "Ellipsometric Study of Ni–P Film Surfaces," *Journal of Applied Physics*, vol. 43, no. 4, pp. 1681-1685, 1972.

[27] S. Pai and J. Marton, "The composition of oxides formed on electroless Ni–P deposits," *J Electrochem Soc*, vol. 120, pp. 1280-1281, 1973.

[28] W. Tomlinson and G. Wilson, "The oxidation of electroless Ni-B and Ni-P coatings in air at 800 to 1000° C," *Journal of materials science*, vol. 21, no. 1, pp. 97-102, 1986.

[29] K. H. Krishnan, S. John, K. Srinivasan, J. Praveen, M. Ganesan, and P. Kavimani, "An overall aspect of electroless Ni-P depositions—A review article," *Metallurgical and materials transactions A*, vol. 37, no. 6, pp. 1917-1926, 2006.

[30] J. Sudagar, J. Lian, and W. Sha, "Electroless nickel, alloy, composite and nano coatings–A critical review," *Journal of alloys and compounds*, vol. 571, pp. 183-204, 2013.

[31] S. Eraslan and M. Ürgen, "Oxidation behavior of electroless Ni–P, Ni–B and Ni–W–B coatings deposited on steel substrates," *Surface and Coatings Technology*, vol. 265, pp. 46-52, 2015.

[32] S. Karthikeyan and L. Vijayaraghavan, "Investigation of the surface properties of heat treated electroless Ni–P coating," *Transactions of the IMF*, vol. 94, no. 5, pp. 265-273, 2016.

[33] P. B. Johnson and R. W. Christy, "Optical constants of transition metals: Ti, V, Cr, Mn, Fe, Co, Ni, and Pd," *Physical Review B*, vol. 9, no. 12, pp. 5056-5070, 06/15/ 1974, doi: 10.1103/PhysRevB.9.5056.

[34] K. Vedam, "Spectroscopic ellipsometry: a historical overview," *Thin Solid Films*, vol. 313-314, pp. 1-9, 1998/02/13/ 1998, doi: https://doi.org/10.1016/S0040-6090(97)00762-1.